Design of a concise and dual-band tunable metamaterial absorber

Zongzhe Li (李宗哲)[1], Chunya Luo (罗春娅)[1], Gang Yao (姚 刚)[1], Jin Yue (乐 进)[1], Jie Ji (季 洁)[1], Jianquan Yao (姚建铨)[1,3], and Furi Ling (凌福日)[2,*]

[1]*Wuhan National Laboratory for Optoelectronics, Huazhong University of Science and Technology, Wuhan 430074, China*

[2]*School of Optical and Electronic Information, Huazhong University of Science and Technology, Wuhan 430074, China*

[3]*College of Precision Instrument and Optoelectronics Engineering, Tianjin University, Tianjin 300072, China*

**Corresponding author: lingfuri@hust.edu.cn*

Received May 27, 2016; accepted August 19, 2016; posted online September 30, 2016

We theoretically present a concise and tunable dual-band metamaterial absorber composed of a typical metal-dielectric-metal structure in the terahertz regime. The dual-band absorption originates from two different resonance modes induced in one square ring, which is different from the common dual-band absorber composed of a super unit with several different-sized structures. The proposed absorber can realize dynamic tunability through changing the permittivity of the dielectric layer by applying different temperatures. Other good performances, such as a wide incident angle and polarization insensitivity, are also available for the proposed absorber. Such a metamaterial absorber is a promising candidate for terahertz imaging and detection.

OCIS codes: 230.0230, 240.02740, 160.0160.

doi: 10.3788/COL201614.102303.

Metamaterials (MMs) consist of a patterned subwavelength metallic unit cell whose electromagnetic properties originate from oscillating electrons. Due to their exotic properties that are unavailable in nature such as negative refractive index[1], perfect lens[2], invisible cloaks[3], and perfect absorption[4], MMs have been extensively studied over the past decade at wavelengths from the visible light to the microwave band. Among many applications of MMs, the perfect MM absorber (PMA) currently has provoked a comprehensive interest owing to its ultrathin and flexible characteristics compared to conventional absorbers.

The first PMA made of a metallic electric ring resonator (ERR) and a cut wire separated by a dielectric layer was proposed by Landy[4], which has realized the experimental absorptivity of 88% at the microwave band. Ever since then, the PMA has attracted intense attention, and a great deal of MM absorbers have been proposed. The operating wavelength extends from the microwave to visible light[4–7] regions. In addition, performances of the PMA have been improved significantly. On the one hand, the absorption band changes from a single band to dual band[8–10], multiband[11–14], and broadband[15–17]. For example, Ma *et al.* proposed a dual-band polarization-insensitive terahertz absorber based on double closed ring[18], Liu *et al.* demonstrated the broadband absorber by using a multilayer stacked structure[12], and Shen *et al.* presented a triple-band absorber[13]. On the other hand, the absorption frequency becomes tunable instead of being fixed. For instance, Padilla *et al.* put forward a liquid crystal tunable PMA[19]. Zhang *et al.* proposed an MM absorber based on a graphene membrane[20]. Wang *et al.* demonstrated a temperature-controlled tunable deep-subwavelength MM absorber[21]. Furthermore, other additive functions like wide incident angle and polarization independency are also achieved in these references[22–25].

In this Letter, we demonstrated a concise dual-band tunable MM absorber with three layers made up of a metallic square ring, a strontium titanate (STO) crystal, and a metallic plate. The dual-band absorption was realized by utilizing the fundamental resonant mode and a new resonant mode existed in the metallic square closed ring. The mechanism of the absorption is explained by electromagnetic dipole resonance. Moreover, compared with the common frequency-fixed absorber, the proposed absorber can easily implement the dynamic absorption frequency by exerting different temperatures on the STO dielectric layer. Furthermore, excellent properties, such as polarization insensitivity, wide incident angle, and deep subwavelength scale (thickness less than $\lambda/30$), are also available for this symmetric structure. We believe that the proposed absorber will be valuable in selective thermal emitters, detectors, and sensors.

The unit cell and array of the proposed absorber are shown in Fig. 1. It can be seen from Fig. 1(b) that the absorber consists of a metallic square ring and substrate separated by a dielectric layer. The top and bottom metal are Au whose conductivity can be treated as constant $\sigma = 4.09 \times 10^7$ Sm^{-1} in the terahertz band[6]. Generally, the material of the middle layer has a low dispersion with almost constant permittivity in the simulated frequency range, such as SiO_2, polymer, and Al_2O_3 etc. However, the intermediate material of the proposed absorber is a thin STO crystal whose permittivity is temperature dependent[26], which is critical to realizing the tunable

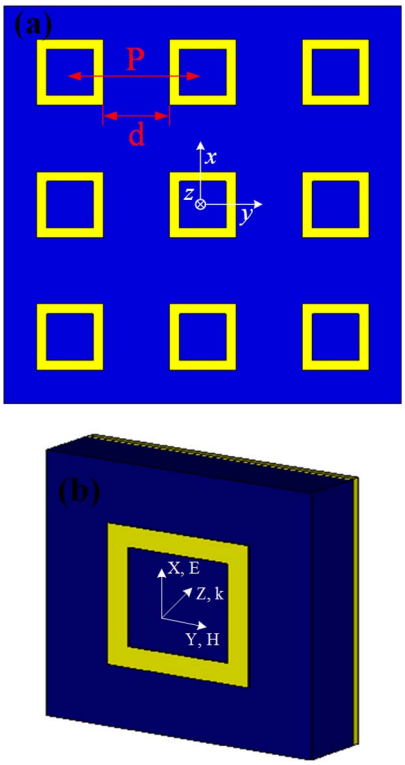

Fig. 1. Schematic of MM absorber. (a) The front view of the MM absorber array, (b) the perspective view of the unit cell.

characteristics of the proposed absorber. We will discuss this in detail in the following chapter.

In our simulation, we used commercial simulation software, the frequency solver of CST Microwave Studio 2011, which is based on the finite element method (FEM). In the boundary condition setup, a unit cell boundary is applied in the x and y directions while an open boundary is assumed to be in the z direction. The propagation direction of the terahertz wave is along the z axis with the electric and magnetic field parallel to the x and y axis, respectively. As shown in Fig. 1(b), the lattice constant is $P = 80$ μm along the x and y direction. The length and width of the square ring are $L = 40$ μm and $W = 6$ μm, respectively. The thickness of the STO is set to 17 μm after optimizing. The thickness of gold is 0.4 μm, much greater than the skin depth of the terahertz wave, which will block the transmission wave. Hence, the absorptance can be obtained by $A = 1 - R - T = 1 - R$ $(T = 0)$, where T, R, and A are the reflectance, transmittance, and absorptance, respectively. By designing the proper parameter of the absorber, the perfect absorption can be realized (i.e., the effective impedance of the absorber is matched to the free space).

Figure 2 shows the calculated absorption spectrum of the proposed absorber at room temperature (300 K). It should be noted that the absorption spectrum contains two obvious absorption peaks located at 0.15 THz (f_{m1}) and 0.30 THz (f_{m2}); the absorptance of the two peaks are 97.97% and 95.92%. The absorption bandwidth,

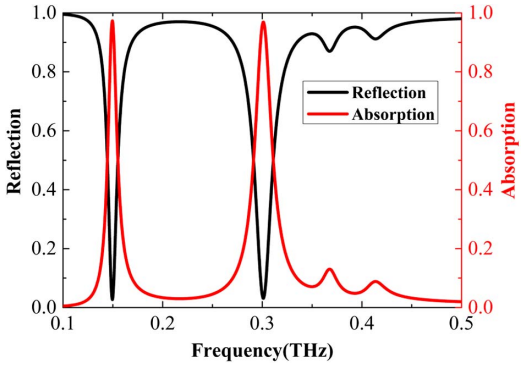

Fig. 2. Calculated absorptance and reflectance spectrum of the proposed absorber at temperature $T = 300$ K.

defined as the full width at half-maximum (FWHM), are 0.01 and 0.02 THz, respectively.

In order to understand the nature of absorption, the distributions of the electric field and magnetic field at two peak frequencies are illustrated in Fig. 3. As shown in Fig. 3(a), it is obvious that the electric field at frequency f_{m1} is mainly concentrated on both sides of the square ring, indicating the existence of an electric dipole resonance on the square ring, as reported by Yao *et al.*[27]. Additionally, the y componenta of the magnetic field at frequency f_{m1} are mainly focused on the middle of STO layer, which means that there exists a magnetic dipole resonance[28], as shown in Fig. 3(c). The resonant phenomenon at low frequency f_{m1} is the fundamental electromagnetic dipole resonance that appeared in some literature[15,21,27–29]. As for the frequency f_{m2}, it can be seen from Figs. 3(b) and 3(d) that the electric field is distributed not only on both inner ends of the square ring but also on the adjacent area between the unit cell; the y component of the magnetic field gathers in the middle and both sides of the STO dielectric layer, which indicates that there exists two kinds of different magnetic dipole resonance. Referring to the similar report[28,29], we deduce that the resonance absorption at high frequency f_{m2} is caused by a new coupled mode, which combines the fundamental electromagnetic dipole mode with the electromagnetic mode caused by the neighboring square ring. We will discuss this in detail later when analyzing the influence of the geometric parameter.

To further reveal the underlying mechanism of absorption quantitatively, we restored the relative effective impedance of the proposed absorber according to the equation[30,31]

$$Z_{\text{eff}} = \sqrt{\frac{(1+S_{11})^2 - S_{21}^2}{(1-S_{11})^2 - S_{21}^2}}, \tag{1}$$

where S_{11} and S_{21} are the scattering parameter, i.e., complex reflection and transmission coefficients. The retrieved relative effective impedance is normalized to the impedance of free space. The real and imaginary parts of the impedance are plotted in Fig. 4. For the first absorption

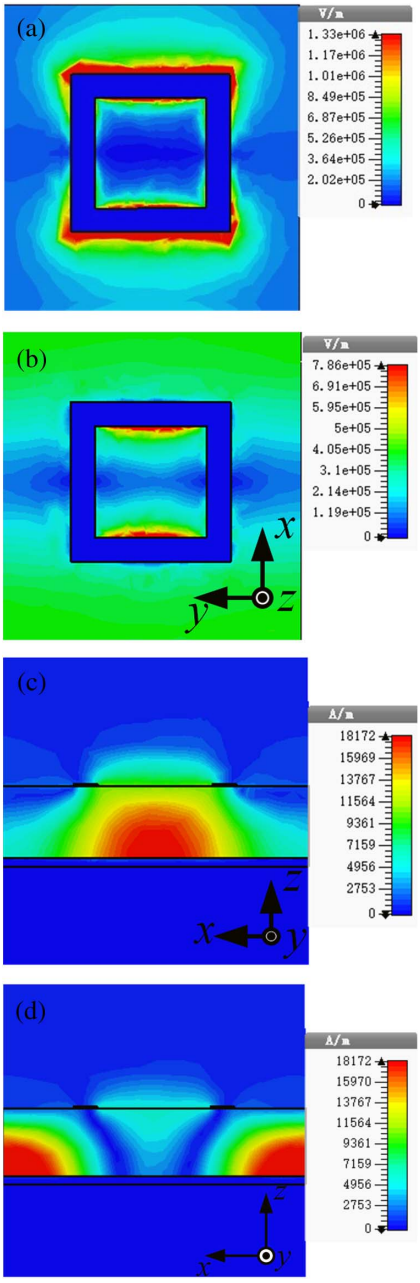

Fig. 3. Distributions of the electric field in the cross section of $z = 17.4$ μm at (a) 0.15 THz (f_{m1}) and (b) 0.3 THz (f_{m2}); distributions of the y component of the magnetic fields in the cross section of $y = 0$ μm at (c) 0.15 THz (f_{m1}) and (d) 0.30 THz (f_{m2}).

peak at 0.15 THz (f_{m1}), the relative effective impedance $Z_{\text{eff1}} = 0.718 + 0.006i$; for the second absorption peak at 0.3 THz (f_{m2}), the relative effective impedance $Z_{\text{eff2}} = 0.700 + 0.015i$. The real part of the impedances of both absorption peaks is close to one while the imaginary part is nearly zero, which means the low reflection (i.e., high absorption) is in accordance with the impedance matching theory[4].

The tunability of the proposed dual-band absorber was further investigated by changing the geometric parameter of the structure. The influence of various lengths on the absorption spectrum is shown in Fig. 5(a). It can be seen

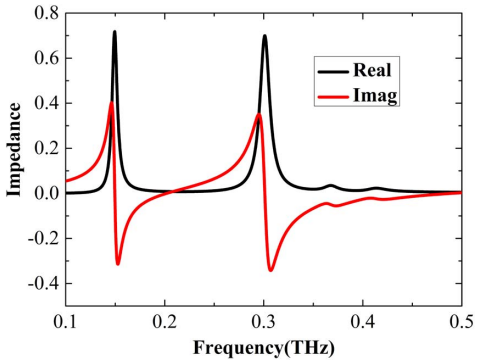

Fig. 4. Real part and imaginary part of the retrieved relative effective impedance at 300 K (normalized to free space impedance).

from Fig. 5(a) that the frequency f_{m1} shifts toward a lower frequency with increasing of the length of the square ring, but the frequency f_{m2} remains unchanged. For the electromagnetic dipole resonance, the LC circuit model is quite suitable for predicting the resonant frequency qualitatively[32]. The formula of the LC circuit model can be obtained by[33]: $f_m = 1/(2\pi\sqrt{LC/2}) \propto 1/(l_{\text{eff}}\sqrt{\varepsilon_r})$, where l_{eff} is the effective oscillating length of the dipole and ε_r is the relative permittivity of the STO. Hence, the redshift phenomenon for resonant frequency f_{m1} can be easily understood according to the LC circuit model where resonant frequency is inversely proportional to effective oscillating length l_{eff}, which is proportional to the length of the square ring. However, as mentioned before, the second resonant frequency f_{m2} is caused by the coupling of the fundamental electromagnetic dipole resonance and the electromagnetic dipole resonance of the neighboring unit cell. According to the LC model, on the one hand, the neighboring-unit resonance mode pushes the frequency f_{m2} toward higher frequencies owing to the narrowing distance of neighboring unit d, i.e. the oscillating length l_{eff} decreases, as shown in Fig. 1(a). On the other hand, the fundamental resonance mode attracts frequency f_{m2} to a lower frequency. So the total result is that the coupling of the two modes keeps the frequency f_{m2} unchanged.

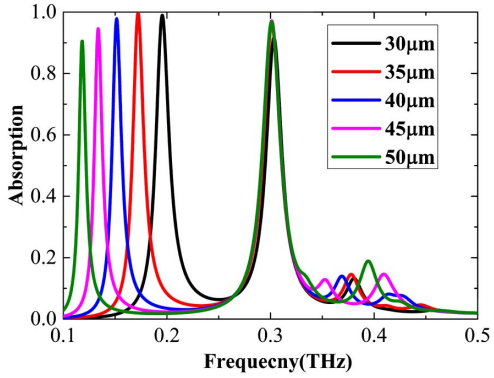

Fig. 5. Absorption spectra for different lengths (unit μm) of square at 300 K.

Although the resonance frequency can be tuned by changing the geometric size of the square ring, it is still an unfeasible way for a fixed structure to revise its geometric dimension. As mentioned before, the permittivity of the dielectric STO can be dynamically tuned by applying different temperatures on the STO, which provides another simple way to achieve agile tuning of the resonance frequency. The permittivity of the STO is plotted in Fig. 6 according to the equations in references[26,34]. It can be seen from Fig. 6(a) that the real part Re(ε) of the STO decreases with increasing of the temperature T. However, at each fixed temperature the dispersion is very small. Conversely, the loss tangent of the permittivity (i.e., the loss tan δ) is insensitive to the temperature, and it is less than 0.08 in the frequency of interest, as shown in Fig. 6(b). These special characteristics of permittivity lead to the tuning of the resonance absorption frequency, which will be analyzed later on.

Figure 7(a) displays the absorption spectra at several different temperatures T (from 200 to 400 K). The resonance frequencies of two absorption peaks undergo a gradual redshift simultaneously as well as maintaining more than 90% absorption. The tuning ranges of peak I and peak II are about 52% and 80%, respectively, compared to the central resonance frequency at 300 K. These results show that our absorber has a performance of good dynamic tuning with temperature. To get further insight on the underlying mechanism of frequency shift, the

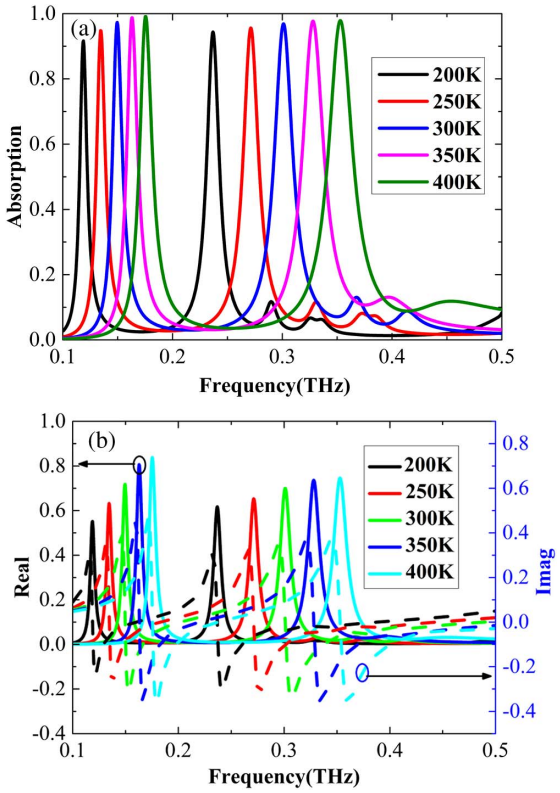

Fig. 7. (a) Absorption spectrum and (b) the retrieved effective impedance at different temperatures (200 to 400 K). The real part is expressed by the solid line, and the imaginary part is indicated by the dotted line.

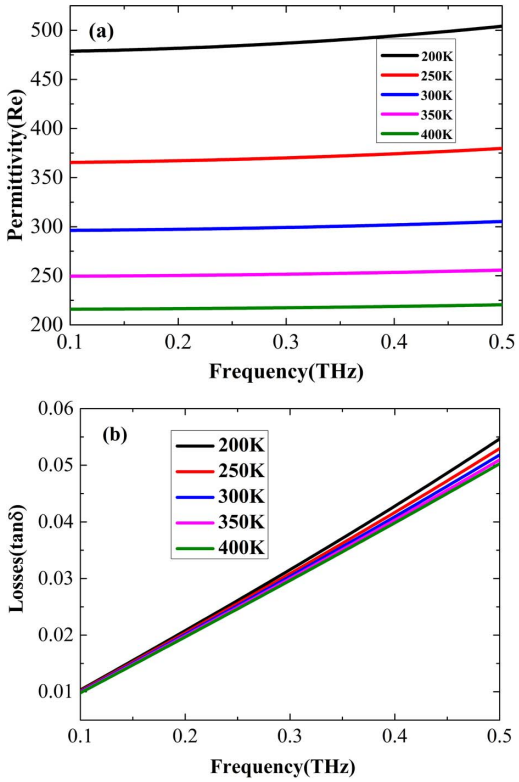

Fig. 6. Permittivity of the STO single crystal at different temperatures (from 200 to 400 K). (a) Real part of permittivity and (b) the loss tangent of permittivity (tanδ).

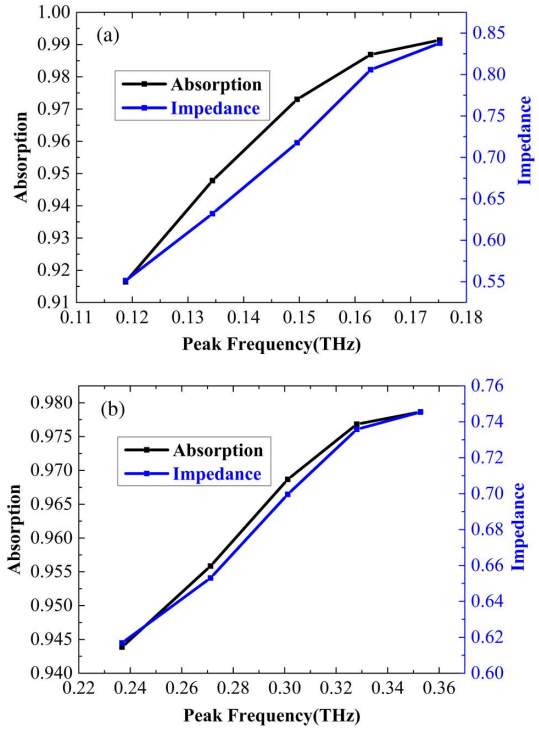

Fig. 8. Absorption and impedance at (a) peak frequency f_{m1} and (b) peak frequency f_{m2} with the temperature increasing from 200 to 400 K.

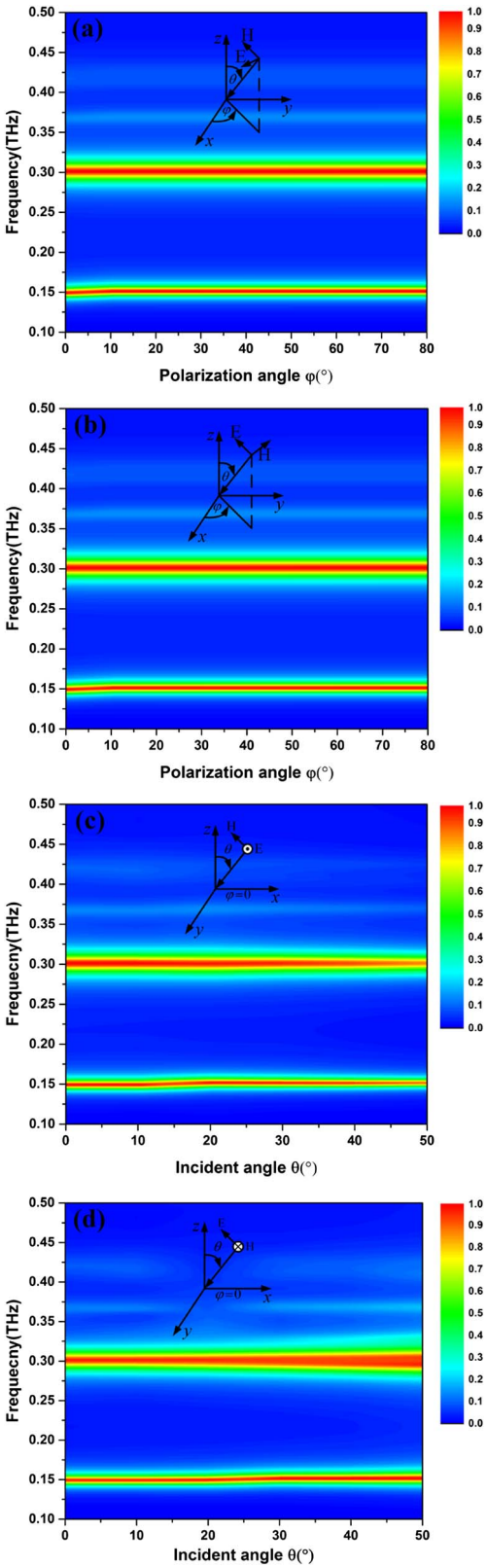

Fig. 9. Absorption spectra as a function of azimuthal angle φ for (a) TE polarization and (b) TM polarization, when incident angle $\theta = 0$; absorption spectra with different incident angles θ for (c) TE polarization and (d) TM polarization, when azimuthal angle $\varphi = 0$.

relative effective impedances at different temperatures are shown in Fig. 7(b). The real parts of the relative effective impedances at peak frequency f_{m1} and peak frequency f_{m2} are always the maximum value (close to one) with change of temperature, but the imaginary part is almost zero. It indicates the impedances of the absorber at peak frequency f_{m1} and f_{m2} are matched to free space[35], which results in the perfect absorption. Hence, the frequency shift can be attributed to the temperature-dependent permittivity that results in the relative effective impedance of the absorber matched to the free space impedance in different resonance frequencies at various temperatures. In order to explain the mechanism explicitly, the relationship between impedance and absorption at peak frequencies f_{m1} and f_{m2} at different temperatures are shown in Figs. 8(a) and 8(b). For peak frequency f_{m1}, the tendency of enhanced absorption for different temperatures is in agreement with the relative effective impedances. For peak frequency f_{m2}, the trend is the same as f_{m1}. According to the impedance matching theory, better matching to free space leads to lower reflectance and higher loss, and it exactly explains the enhancement of absorption with increasing temperature T in Fig. 7(a). Except for the good tunability property, the proposed absorber is also polarization independent for both TE and TM polarization due to its four-fold symmetry, as shown in Figs. 9(a) and 9(b). Furthermore, as shown in Figs. 9(c) and 9(d), the absorption can stay more than 80% even when the incident angle increases to 50° in both the TE and TM configuration, which implies the good property of a wide incident angle.

In conclusion, we present a temperature-controlling dual-band MM absorber in the terahertz band composed of a metallic square ring and a metallic mirror plane separated by an STO dielectric layer. Dual-band absorption is achieved by a simple square ring instead of a traditional complex two-square ring. The mechanisms of the two absorption peaks are quite distinct. The low frequency f_{m1} is the common fundamental electromagnetic resonance (fundamental mode), however, the high frequency f_{m2} is a new resonant mode that originated from the coupling of the fundamental mode and electromagnetic resonance of the adjacent unit. In addition, the tuning range of the two peaks are 52% and 80% when the temperature changes from 200 to 400 K. The tunability is attributed to the change of permittivity of the STO, which leads to the relative effective impedance of the absorber matched to the free space impedance at different resonant frequencies for different temperatures. Moreover, the properties of polarization independence and wide incident angle can also be realized in this symmetric structure. The proposed absorber can be applied to tunable terahertz devices, thermal emitters, and terahertz imaging systems.

This work was supported by the National Basic Research Program of China (No. 2015CB755403), the CAEP THz Science and Technology Foundation (No. AEPTHZ201402), and the CAEP THz Science and Technology Foundation (No. AEPTHZ201407).

References

1. W. J. Padilla, D. N. Basov, and D. R. Smith, Mater. Today **9**, 28 (2006).
2. J. B. Pendry, Phys. Rev. Lett. **85**, 3966 (2000).
3. D. Schurig, J. J. Mock, B. J. Justice, S. A. Cummer, J. B. Pendry, A. F. Starr, and D. R. Smith, Science **314**, 977 (2006).
4. N. I. Landy, S. Sajuyigbe, J. J. Mock, D. R. Smith, and W. J. Padilla, Phys. Rev. Lett. **100**, 207402 (2008).
5. N. Liu, M. Mesch, T. Weiss, M. Hentschel, and H. Giessen, Nano Lett. **10**, 2342 (2010).
6. Y. Q. Ye, Y. Jin, and S. He, J. Opt. Soc. Am. B **27**, 498 (2010).
7. K. Aydin, V. E. Ferry, R. M. Briggs, and H. A. Atwater, Nat. Commun. **2**, 517 (2011).
8. J. Yu, H. Chen, X. Yu, and S. Liu, Chin. Opt. Lett. **12**, S11301 (2014).
9. Q.-Y. Wen, H.-W. Zhang, Y.-S. Xie, Q.-H. Yang, and Y.-L. Liu, Appl. Phys. Lett. **95**, 241111 (2009).
10. Y. Li, B. Wang, X. Xu, and L. Su, Chin. Opt. Lett. **12**, 101603 (2014).
11. J. Grant, I. J. McCrindle, C. Li, and D. R. Cumming, Opt. Lett. **39**, 1227 (2014).
12. S. Liu, J. Zhuge, S. Ma, H. Chen, D. Bao, Q. He, L. Zhou, and T. J. Cui, J. Appl. Phys. **118**, 014909 (2015).
13. X. Shen, Y. Yang, Y. Zang, J. Gu, J. Han, W. Zhang, and T. J. Cui, Appl. Phys. Lett. **101**, 154102 (2012).
14. H. Li, L. H. Yuan, B. Zhou, and X. P. Shen, J. Appl. Phys. **110**, 014909 (2011).
15. Y. J. Kim, Y. J. Yoo, K. W. Kim, J. Y. Rhee, Y. H. Kim, and Y. Lee, Opt. Express **23**, 3861 (2015).
16. S. Liu, H. Chen, and T. J. Cui, Appl. Phys. Lett. **106**, 163702 (2015).
17. X. X. Tian and Z. Y. Li, Photon. Res. **4**, 146 (2016).
18. Y. Ma, Q. Chen, J. Grant, S. C. Saha, A. Khalid, and D. R. Cumming, Opt. Lett. **36**, 945 (2011).
19. D. Shrekenhamer, W.-C. Chen, and W. J. Padilla, Phys. Rev. Lett. **110**, 177403 (2013).
20. Y. Zhang, Y. Feng, B. Zhu, J. Zhao, and T. Jiang, Opt. Express **22**, 22743 (2014).
21. B.-X. Wang, X. Zhai, G.-Z. Wang, W.-Q. Huang, and L.-L. Wang, Opt. Mater. Express **5**, 227 (2015).
22. Y. Avitzour, Y. A. Urzhumov, and G. Shvets, Phys. Rev. B **79**, 045131 (2009).
23. Y. Q. Xu, P. H. Zhou, H. B. Zhang, L. Chen, and L. J. Deng, J. Appl. Phys. **110**, 044102 (2011).
24. X. Shen, T. J. Cui, J. Zhao, H. F. Ma, W. X. Jiang, and H. Li, Opt. Express **19**, 9401 (2011).
25. B. Zhang, Y. Zhao, Q. Hao, B. Kiraly, I.-C. Khoo, S. Chen, and T. J. Huang, Opt. Express **19**, 15221 (2011).
26. P. Kužel and F. Kadlec, C. R. Phys. **9**, 197 (2008).
27. G. Yao, F. Ling, J. Yue, C. Luo, J. Ji, and J. Yao, Opt. Express **24**, 1518 (2016).
28. B.-X. Wang, X. Zhai, G.-Z. Wang, W.-Q. Huang, and L.-L. Wang, J. Appl. Phys. **117**, 014504 (2015).
29. Z.-C. Xu, R.-M. Gao, C.-F. Ding, L. Wu, Y.-T. Zhang, and J.-Q. Yao, Opt. Mater. **42**, 148 (2015).
30. D. Smith, S. Schultz, P. Markoš, and C. Soukoulis, Phys. Rev. B **65**, 195104 (2002).
31. D. Smith, D. Vier, T. Koschny, and C. Soukoulis, Phys. Rev. E **71**, 036617 (2005).
32. L. Min and L. Huang, Opt. Express **23**, 19022 (2015).
33. J. Zhou, E. N. Economon, T. Koschny, and C. M. Soukoulis, Opt. Lett. **31**, 3620 (2006).
34. V. Skoromets, F. Kadlec, C. Kadlec, H. Němec, I. Rychetsky, G. Panaitov, V. Müller, D. Fattakhova-Rohlfing, P. Moch, and P. Kužel, Phys. Rev. B **84**, 174121 (2011).
35. Y. Ma, H. Zhang, Y. Li, and Y. Wang, J. Opt. Soc. Am. B **31**, 325 (2014).